


## Reexamining the Stark width and shift of He II Paschen- $\alpha$ : Studies using laser-induced plasma, Thomson scattering, and computer simulations

Krzysztof Dzierżęga<sup>✉,\*</sup>, Franciszek Sobczuk<sup>†</sup>, and Tomasz Krehlik<sup>‡</sup>

*Marian Smoluchowski Institute of Physics, Jagiellonian University, ul. Łojasiewicza 11, 30-348 Kraków, Poland*

Evgeny Stambulchik<sup>✉,§</sup>

*Faculty of Physics, Weizmann Institute of Science, Rehovot 7610001, Israel*

 (Received 31 January 2024; accepted 24 May 2024; published 27 June 2024)

We report on experimental and theoretical studies on the Stark profile of the He II Paschen- $\alpha$  line over a wide range of plasma parameters. This line was emitted from a laser-induced plasma with electron densities in the range of  $8.1 \times 10^{22}$ – $4.46 \times 10^{24}$  m<sup>-3</sup> and electron temperatures of 1.2–7.6 eV as independently measured using the two-color Thomson scattering method. The line shapes were calculated using a computer simulation method, treating the ions and electrons on an equal footing and taking into account the full Coulomb interaction between the hydrogenlike atomic radiator and plasma perturbers penetrating the wave-function extent of the bound electron. We found a very good agreement between the experimental and theoretical Stark widths and shifts, which on average agree within 5%. In addition, practical analytical approximations for the linewidth and line shift are provided, validated against extensive calculations in the density and temperature ranges of  $10^{23}$ – $10^{25}$  m<sup>-3</sup> and 1–16 eV, respectively.

DOI: [10.1103/PhysRevE.109.065214](https://doi.org/10.1103/PhysRevE.109.065214)

### I. INTRODUCTION

Stark profiles (in particular, their widths and shifts) of spectral lines are widely used in laboratory plasma diagnostics and astrophysical research. Among them, transitions in hydrogen and hydrogenlike ions are particularly important because of the simplicity of their one-electron atomic system and abundance in space. Plasma broadening of the He II Paschen- $\alpha$  line (a transition between levels with the principal quantum number  $n = 4$  and  $n = 3$  of a singly ionized helium atom) has been studied for a long time. Although the plasma-induced width of the line generally agrees with the results of many studies, the same cannot be said for its shift: There is a significant spread of available experimental results and, until recently, the theoretical values of the shift were systematically below the best experimental ones [1–6]. It has recently been shown [7], however, that these discrepancies can be resolved by accounting for the full Coulomb interaction between the radiating helium ion and plasma perturbers (electrons and ions). In particular, the monopole radiator-plasma interaction term was found to be primarily responsible for the additional Stark shift that was missing in earlier calculations.

Here, we significantly extend the study of the He II Paschen- $\alpha$  Stark profile [7] by investigating it over a wide range of electron densities and temperatures. For plasma diagnostics, the recently developed two-color Thomson scattering

(TS) method [8] is used, employing the second and third harmonics of an Nd:YAG laser as probing beams, with the plasma parameters derived based on the electron or ion features of the TS spectra. In order to increase the precision of determining the plasma-induced line shift, a tunable Ti:sapphire continuous-wave (cw) laser with a second-harmonic generator and a wavemeter are used to calibrate the wavelength scale. As in the previous study, line-shape calculations [9] are performed for the plasma parameters derived.

### II. EXPERIMENT

The experimental setup is shown schematically in Fig. 1. A vacuum chamber was evacuated below  $10^{-5}$  mbar and then filled with pure helium at a pressure in the range of 300–2000 mbar. Plasma was created in the center of the chamber by focusing a second-harmonic ( $\lambda = 532$  nm) Q-switched Nd:YAG laser pulse (4.5 ns duration, 10 Hz repetition rate, and energy of 115 mJ) using a 50-mm focal length aspheric lens. The laser spot of about 46  $\mu$ m in diameter resulted in a laser fluence estimated at 2.4 kJ/cm<sup>2</sup>. For plasma diagnostics using the Thomson scattering method, another nanosecond Nd:YAG but single-mode ( $\delta\lambda < 0.5$  pm) laser was used together with the second- and third-harmonic generators. The resulting pulses of 532 and 355 nm, to avoid plasma heating effects, were attenuated to energies of 1 and 4 mJ, respectively, with the use of Rochon prisms and half-wave plates. These probe laser beams, focused onto spots of about 60  $\mu$ m in diameter in the plasma volume, propagated orthogonally to the pump beam and were polarized perpendicularly to the direction of observation. A digital pulse generator controlled the delay between the pump and probe pulses.

\*Contact author: [krzysztof.dzierzega@uj.edu.pl](mailto:krzysztof.dzierzega@uj.edu.pl)

†Contact author: [franciszek.sobczuk@doctoral.uj.edu.pl](mailto:franciszek.sobczuk@doctoral.uj.edu.pl)

‡Contact author: [tomasz.krehlik@doctoral.uj.edu.pl](mailto:tomasz.krehlik@doctoral.uj.edu.pl)

§Contact author: [evgeny.stambulchik@weizmann.ac.il](mailto:evgeny.stambulchik@weizmann.ac.il)

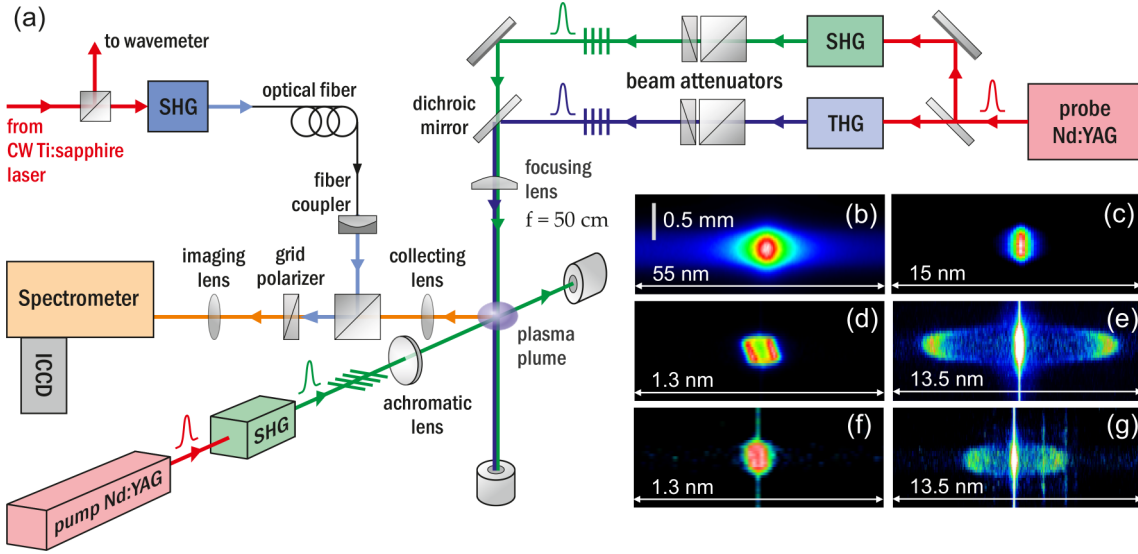


FIG. 1. (a) The experimental setup. Images of plasma emission spectra containing the He II Paschen- $\alpha$  line [(b), (c)] and of Thomson scattering spectra at 532 nm [(d), (e)] and 355 nm [(f), (g)] probe beams, recorded for pressure  $p = 2000$  mbar and delay  $\Delta t = 30$  ns [(b), (d), (f)] and  $p = 500$  mbar and  $\Delta t = 90$  ns [(c), (e), (g)]. The white color in the images of the Thomson scattering spectra [(e) and (g)] does not mean the saturation of the ICCD but results from scaling the intensities to observe both the electron and ion features. Only the ionic features [(d), (f)] were registered in the second case, since the electron ones disappeared in the photon noise.

Plasma emission and laser-scattered light were observed perpendicularly to laser beams by imaging the investigated area of plasma onto the entrance slit of a Czerny-Turner spectrometer (750 mm focal length, 4.0 or 0.502 nm/mm reciprocal dispersion) equipped with a gated two-dimensional intensified charge-coupled device (ICCD). Instrumental spectral profiles were determined using different cw laser sources and are well approximated by a pseudo-Voigt function with a full width at half maximum (FWHM) of 0.244 nm ( $11.4 \text{ cm}^{-1}$ ). The spectral sensitivity of the optical and detection systems was measured using a calibrated halogen-deuterium lamp. On the other hand, a precise wavelength calibration was performed using the second harmonic of a cw tunable Ti:sapphire laser, the wavelength of which was measured with the use of a wavemeter with an accuracy of 1.0 pm ( $0.05 \text{ cm}^{-1}$ ).

Optical signals for various experimental conditions (see Table I) were acquired with an 8-ns ICCD gate width and averaged over 15000 laser shots. Such a short measurement

time makes the investigated emission spectra originating from a more quasistationary plasma and increases the signal-to-noise ratio of the laser-scattered light. The latter was further improved by inserting the polarizer into the path of the measured light, thus removing the depolarized part of the laser-scattered light and simultaneously attenuating the plasma light.

TS and plasma emission spectra, obtained for plasma induced at pressures of 2000 and 500 mbar, and for delays of 30 and 90 ns, respectively, are shown in Figs. 1(b)–1(g). All of them have already been corrected for the spectral sensitivity of the experimental system and with the ICCD dark current subtracted. Moreover, laser-scattered spectra [Figs. 1(b), 1(d), and 1(f)] are corrected for the plasma continuum background. The plasma emission spectra are laterally integrated, so they are subject to the inverse Abel transformation to recover the radially resolved spectra corresponding to the laser-scattered ones. For plasma diagnostics, depending on physical conditions, either the central (ion feature) or

TABLE I. Experimental conditions, plasma parameters derived using the TS method, and experimental and theoretical Stark shifts and widths of the He II Paschen- $\alpha$  spectral line.

Pressure (mbar)	Delay (ns)	$k_B T$ (eV)	$n_e$ ( $10^{24} \text{ m}^{-3}$ )	$\sigma_e$ (%)	$w^{\text{th}}$ ( $\text{cm}^{-1}$ )	$w^{\text{expt}}$ ( $\text{cm}^{-1}$ )	$d^{\text{th}}$ ( $\text{cm}^{-1}$ )	$d^{\text{expt}}$ ( $\text{cm}^{-1}$ )
2000	30	7.62	4.467	11.2	296.3(14.8)	301.1(1.0)	-31.85(4.78)	-33.34(0.68)
2000	40	6.94	2.780	6.68	200.8(10.0)	202.2(0.8)	-20.49(3.07)	-20.57(0.67)
2000	60	5.17	1.363	7.86	115.1(5.76)	124.80(0.66)	-10.56(1.58)	-11.17(0.66)
2000	100	3.23	0.865	7.39	78.88(3.94)	82.66(0.59)	-7.22(1.08)	-6.69(0.65)
1000	120	2.70	0.343	4.90	40.20(2.01)	42.01(0.25)	-3.27(0.49)	-3.42(0.64)
500	90	2.09	0.188	15.57	25.87(1.29)	27.68(0.14)	-1.81(0.27)	-2.05(0.63)
300	90	1.32	0.08456	2.57	14.23(0.71)	15.69(0.20)	-0.97(0.15)	
300	100	1.20	0.08171	4.59	13.17(0.66)	14.07(0.26)	-0.89(0.13)	

the sideband (electron feature) parts of the TS spectra were utilized.

### III. THEORETICAL MODEL

The calculations presented in this paper are based on the same theoretical model and use the same numerical implementation as recently described [7]. Briefly, the evolution of a radiating atom (here, singly ionized helium) is obtained by numerically solving the time-dependent Schrödinger equation, where the interaction between the radiator and its plasma environment is modeled by molecular-dynamics simulations assuming the classical motion of Debye quasiparticles [9]. The principal improvement of these calculations as compared, for example, to those from Ref. [10], is the evaluation of the *full* radiator-perturber interaction, preserving the monopole interaction. This is contrary to the “standard” multipole expansion, which begins with the dipole term. The monopole term, in particular, is responsible for the plasma polarization shift (PPS) and thus is crucial for reproducing the He II Paschen- $\alpha$  line shift.

The evaluation of the full radiator-perturber interaction is computationally heavy. To reduce the overall complexity of the simulations, only matrix elements between states with the same principal quantum number  $n$  are calculated in the full radiator-perturber interaction model. On the other hand, mixing between states with different  $n$ 's mainly contributes to the quadratic Stark effect, for which the usual dipole approximation provides sufficient accuracy. Thus, the calculations are repeated three times: first, in the usual dipole approximation and the degenerate, nonquenching (i.e., neglecting  $\Delta n \neq 0$  Stark mixing) atomic model; second, the same but allowing for the full radiator-perturber interaction; and finally, in the dipole approximation allowing for all states to interact without any limitations. All states with  $3 \leq n \leq 6$  are included in the latter case.

Compared to the first model, the second one gives the nondipole shift (mostly PPS), resulting in a minor additional width and a very minor asymmetry. These additional width and shift are applied to the line shape obtained in the third model. Thus, the widths and shifts of the final line shape are, respectively,

$$w = (w^{(2)} - w^{(1)}) + w^{(3)} - \Delta_{\text{gr}}/2 \quad (1a)$$

and

$$d = d^{(2)} + d^{(3)}, \quad (1b)$$

where the superscripts refer to the model number. Note that  $d^{(1)} \equiv 0$  [11]. The last term in Eq. (1a) corrects for the finite step of the spectral grid,  $\Delta_{\text{gr}}$ , used in the calculations (the  $1/2$  factor was empirically determined by varying  $\Delta_{\text{gr}}$  and observing the resulting linewidth in a subset of the calculations). The actual value of  $\Delta_{\text{gr}}$  chosen in each case is based on the balance between the desired accuracy and computational resources available; requirements for the latter grow steeply with decreasing  $\Delta_{\text{gr}}$  [10].

Following the same evaluation principles as those outlined in Ref. [7], the uncertainties in the theoretical width and shift values are believed to be 5% and 15%, respectively.

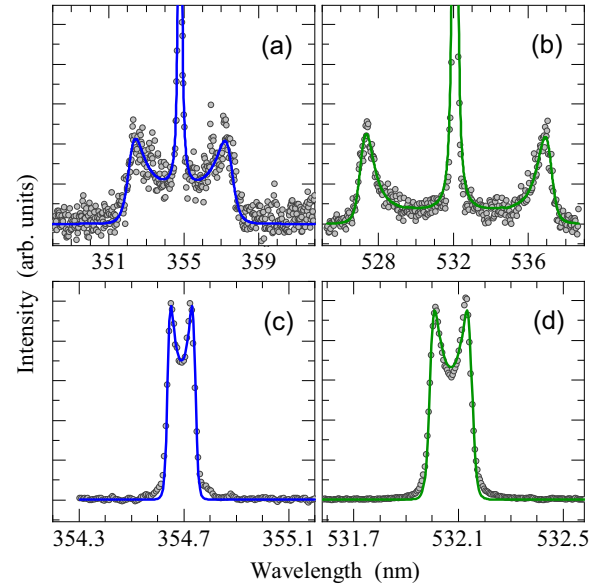


FIG. 2. Thomson scattering spectra recorded with probe lasers at (a), (c) 355 nm and (b), (d) 532 nm at different experimental plasma conditions: (a), (b) 500 mbar and 90 ns delay, and (c), (d) 2000 mbar and 30 ns. The solid lines represent spectral density functions as fitted simultaneously to the spectra measured with both probe lasers.

### IV. RESULTS

The principal plasma parameters, the electron density ( $n_e$ ) and plasma temperature ( $T$ ), were determined by fitting the spectral density function, convolved with the instrumental profile, simultaneously to the ion or electron features of both TS spectra, that is, recorded with 355- and 532-nm probe lasers. In the case of the two shortest delays (30 and 40 ns), the ionic parts were used, while in the remaining cases the electronic features were studied. It should be emphasized that, unlike optical emission spectroscopy, the results do not depend on assumptions about plasma thermodynamic equilibrium, chemical composition, or the selected plasma model. Details on the Thomson scattering technique and its application to the investigation of laser-induced plasma and plasma Stark profiles of spectral lines can be found in Refs. [8,12–14]. Unlike the standard analysis of the TS spectra observed in the case of laser-induced plasmas, we consider the distribution of  $n_e$  originating from plasma heterogeneity, its evolution over the measured interval, and its shot-to-shot variability. All these effects were included in the fitted spectral density function with  $n_e$  subject to a normal distribution with variance  $\sigma_e$ . At the same time, variations in  $T$  were neglected, assuming their minor impact on TS spectra.

Figure 2 shows the fits of the TS spectral density function with the measured TS spectra for the experimental conditions of 2000 mbar pressure and 30 ns delay and of 500 mbar and 90 ns. The values of  $n_e$ ,  $\sigma_e$ , and  $T$  determined by the TS method under the experimental conditions studied and in the axial region of the plasma are presented in Table I. The electron density changes almost 60 times, while the plasma temperature changes only about sixfold, i.e., from  $8.2 \times 10^{22}$  to  $4.5 \times 10^{24} \text{ m}^{-3}$  and from 1.2 to 7.62 eV, respectively.

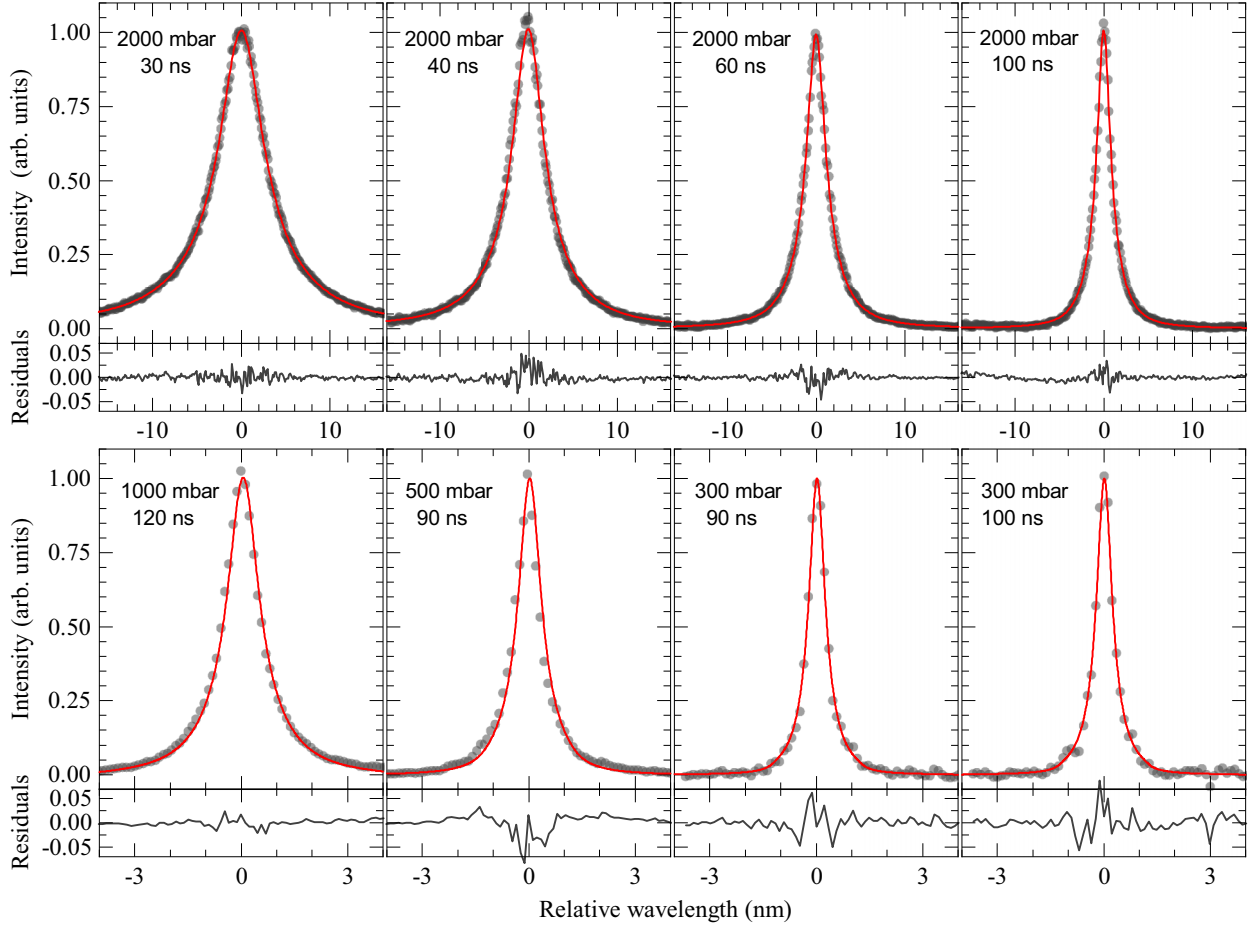


FIG. 3. Superimposed experimental and theoretical line profiles at various plasma conditions. The latter profiles are computer-simulated convolved with the instrumental and Doppler profiles. The zero wavelength corresponds to the positions of the maxima of both the experimental and theoretical profiles.

The respective radially resolved He II Paschen- $\alpha$  line profiles were determined by applying the inverse Abel transform to the measured laterally integrated intensity distributions. These spectra are then fitted by a sum of a Voigt function and a linear function. The latter represents contributions from the plasma continuum and far wings of neighboring spectral lines.

The effects of the density distribution on the theoretical line shapes were accounted for [15], resulting in minor ( $\lesssim 1\%$ ) corrections to the linewidths and shifts. Finally, the theoretical profiles were convolved with the instrumental broadening and the Doppler broadening, the latter ranging from 0.020 to 0.050 nm (from 0.91 to 2.27  $\text{cm}^{-1}$ ).

A comparison between all measured and calculated line shapes is given in Fig. 3, with their Stark widths and shifts separately compared in Figs. 4 and 5. These results show very good agreement between the measured and computer-simulated line profiles in the entire range of plasma conditions attained in the experiment. The discrepancies between the experiment and the theory for linewidths and shifts are, on average, around 5%.

## V. DISCUSSION

Our results on the Stark width of Paschen- $\alpha$  for low ( $\lesssim 5 \times 10^{23} \text{ m}^{-3}$ ) electron densities are comparable with those

calculated according to a semiempirical formula given by Pittman and Fleurier [2]. However, the agreement worsens at higher  $n_e$ , with the discrepancy becoming as high as 30% for the highest electron densities studied in this work (see Fig. 5). The line shift increases almost linearly with  $n_e$ , and the results of our experiment are very well reproduced by the formula given by Gawron *et al.* [4].

As is evident from the data in Table I and observed in Fig. 4, within the scope of the experimental conditions, the linewidth and line shift vary with electron density  $\propto n_e^{0.75(1)}$  and  $\propto n_e^{0.95(3)}$ , respectively. However, the analysis based on the experimental data is not straightforward because successive electron densities correspond to different plasma temperatures. Therefore, to analyze the dependence on  $n_e$  and  $T$  separately, additional systematic calculations were performed on a grid of  $n_e$  from  $10^{23}$  to  $10^{25} \text{ m}^{-3}$  and  $k_B T$  from 1 to 16 eV.

The necessary ionization stage populations were calculated by assuming an optically thin plasma slab in the collisional-radiative equilibrium. In a low-temperature ( $k_B T \sim 1 \text{ eV}$ ) steady-state plasma, the populations of excited He II levels are negligible, and the Paschen- $\alpha$  line is practically impossible to observe. However, in a moderately low-density ( $n_e \lesssim 10^{24} \text{ m}^{-3}$ ), initially hot transient plasma, it may take a significant time to reach equilibrium level populations, so that the

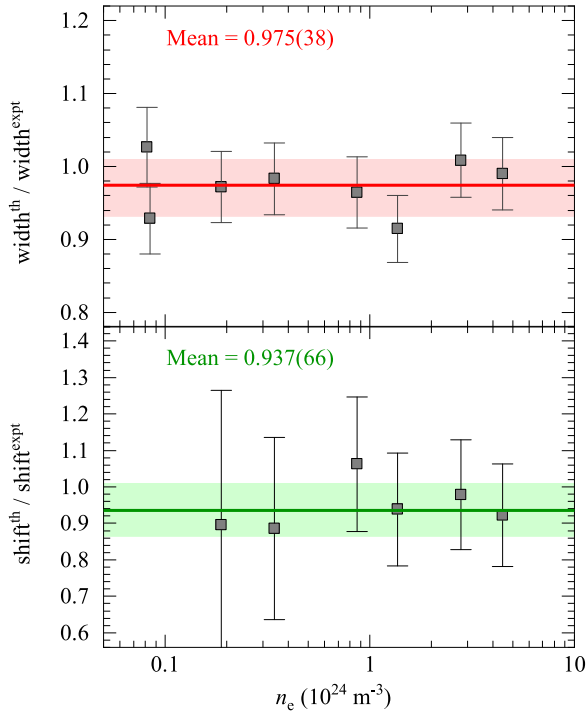


FIG. 4. Ratios of the theoretical to experimental results vs electron density.

Paschen- $\alpha$  emission remains detectable, which is confirmed by our experiments.

To minimize uncertainties due to computational noise on the inferred linewidth and line shift, they are determined as a weighted Lorentzian that best fits the computer-simulated line shape  $L(\omega)$ . The fitting weights  $\propto L(\omega)^4$  were chosen to decrease the influence of any asymmetry in the line wings.

The results—linewidths and line shifts—of these calculations are shown in Table II and Fig. 6. Note that these data correspond to the normalized line shape widely used in line-broadening theory without the so-called “trivial” corrections. The latter are briefly reviewed in Sec. VI.

As can be observed, the major contribution to the width is the linear Stark effect (the “dipole degenerate” model). Its reduction due to both the penetrating collisions and the additional broadening caused by the nondipole terms are minor and partially cancel out, with the net effect (the difference between “dipole degenerate” and “full degenerate”) on the order of a few percent. However, with increasing  $n_e$ , the nonlinear (mainly quadratic) dipole Stark effect due to the mixing of states with different  $n$ 's (the difference between “dipole” and “dipole degenerate”) becomes increasingly important. Both plasma electrons and ions contribute to the linewidth, but in different ways. Specifically, electron broadening has an impact character across the entire range of plasma parameters, with  $w \propto n_e T^{-1/2}$  [16], whereas ion broadening is more complex. That is, unlike the line wings correctly described within the quasistatic approximation, the central part of the line profile is significantly influenced by the unshifted (strictly so in the degenerate dipole approximation) Stark component. The broadening of this central component is well described by the rotational approximation [17] with  $w \propto n_i^{1/3} T^{1/2}$ .

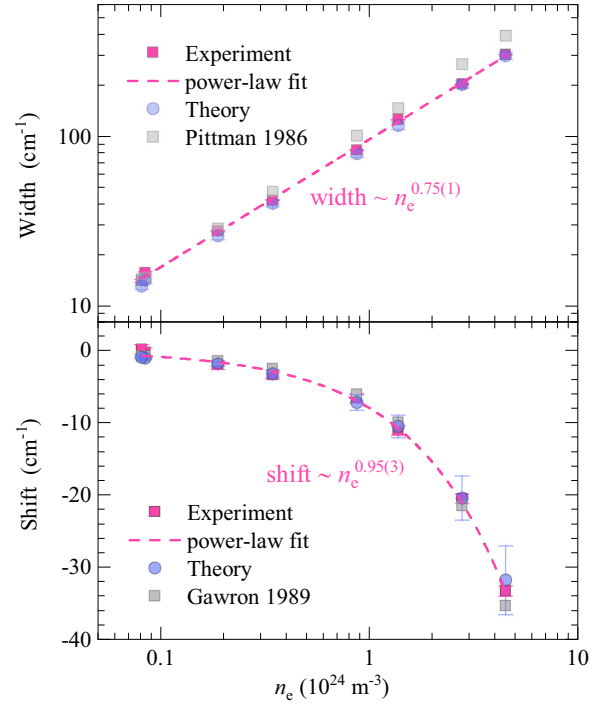


FIG. 5. Experimental and theoretical Stark widths and shifts vs electron density. Also shown are power-law fits of the experimental values and semiempirical results for the width and shift given by Pittman and Fleurier [2] and Gawron *et al.* [4], respectively.

At the lowest  $n_e$  and  $T$  considered here, the contributions of electrons and ions to the linewidth are comparable. They change proportionally to  $T^{-1/2}$  and  $T^{1/2}$ , respectively, but their sum still increases with plasma temperature. As  $n_e$  increases, the influence of electrons on linewidth becomes more significant than that of ions. This applies to the central part where the electron impact varies  $\propto n_e$  vs  $\propto n_i^{1/3}$  for the component rotationally broadened by ions, as well as to the line wings and “shoulders” where the quasistatic approximation holds for the ions that produce  $w \propto n_i^{2/3}$ . As a result, the temperature dependence becomes weaker and even changes sign [18] at the highest density. Combining these different linewidth dependencies on  $n_e$  and  $T$  results in an overall effective relationship that, by chance, is close to the quasistatic one. The same accidental relationship was previously reported for the Lyman- $\alpha$  line [17].

Unlike the linewidth, the  $\Delta n = 0$  and  $\Delta n \neq 0$  contributions to the shift are comparable across the entire range of plasma parameters (see Fig. 6). Not surprisingly, the PPS effect decreases monotonically with increasing temperature: The higher  $T$ , the smaller is the spatial displacement of the electron and ion clouds formed around the charged radiator. The shift due to the nonlinear Stark effect is also nearly monotonously decreasing as a function of temperature at the lowest density considered. However, this dependence is partially offset by an increase in the microfields towards higher  $T$  due to the weakening of the Debye screening: The higher  $n_e$ , the more important Debye screening becomes, and thus this contribution to the line shift becomes monotonously increasing at the highest density.

TABLE II. Results of the calculations on a plasma temperature and density grid. The width ( $w$ ) and shift ( $d$ ) calculated within different models are shown, as well as the spectral grid ( $\Delta_{\text{gr}}$ ) used in the simulations. The “combined” values are calculated according to Eq. (1). All values are in units of  $\text{cm}^{-1}$ .

$k_B T$ (eV)	$\Delta_{\text{gr}}$	Dipole degenerate		Full degenerate		Dipole		Combined	
		$w$	$d$	$w$	$d$	$w$	$d$	$w$	$d$
$n_e = 10^{23} \text{ m}^{-3}$									
1	0.308	14.6	15.1	-0.505	15.4	-0.709	15.7	-1.21	
2	0.308	16.0	16.3	-0.376	16.8	-0.659	17.0	-1.03	
4	0.307	17.8	18.1	-0.337	18.6	-0.605	18.7	-0.942	
8	0.280	19.9	20.2	-0.329	21.1	-0.574	21.3	-0.904	
16	0.280	22.8	22.7	-0.338	24.0	-0.449	23.8	-0.787	
$n_e = 3 \times 10^{23} \text{ m}^{-3}$									
1	0.444	29.9	31.5	-1.52	33.8	-1.73	35.1	-3.25	
2	0.444	31.0	32.0	-1.10	34.9	-1.82	35.7	-2.91	
4	0.443	34.0	34.9	-0.983	38.7	-1.65	39.4	-2.63	
8	0.404	36.9	37.4	-0.936	42.1	-1.49	42.4	-2.43	
16	0.403	41.4	42.2	-1.05	47.3	-1.30	47.9	-2.35	
$n_e = 10^{24} \text{ m}^{-3}$									
1	0.663	68.6	72.3	-4.85	80.8	-4.85	84.2	-9.70	
2	0.663	69.2	71.9	-3.77	84.2	-5.03	86.6	-8.81	
4	0.662	72.7	73.7	-3.50	89.9	-4.76	90.5	-8.26	
8	0.604	75.6	76.6	-3.13	95.6	-4.64	96.3	-7.77	
16	0.603	82.6	83.5	-3.26	104	-4.25	105	-7.52	
$n_e = 3 \times 10^{24} \text{ m}^{-3}$									
1	0.957	156	164	-14.2	191	-11.5	199	-25.7	
2	0.957	152	156	-10.8	195	-12.6	199	-23.4	
4	0.956	153	154	-9.50	204	-13.1	205	-22.6	
8	0.873	151	153	-9.10	215	-12.8	216	-21.9	
16	0.869	161	163	-9.49	230	-12.2	231	-21.7	
$n_e = 10^{25} \text{ m}^{-3}$									
1	1.43	369	386	-39.0	464	-29.1	481	-68.1	
2	1.43	363	375	-33.1	502	-34.3	513	-67.4	
4	1.43	364	367	-31.2	536	-37.8	539	-69.1	
8	1.31	343	339	-26.4	559	-38.4	554	-64.7	
16	1.30	350	348	-29.1	592	-38.6	589	-67.7	

Another minor effect that contributes to this dependence is the change in the mean ion charge  $\langle Z_i \rangle$  in the plasma, which increases from  $\approx 1$  to nearly 2 as  $k_B T$  varies from 1 to 16 eV. As a result, the ion microfields  $\sim \langle Z_i \rangle n_i^{2/3}$  increase as  $\langle Z_i \rangle^{1/3}$  at a constant  $n_e$ . The total line shift, which in this model is a sum of these two contributions, decreases monotonously with temperature. However, the rate of this decline decreases with increasing  $n_e$  and stops for the highest densities investigated.

Since the developed theoretical model reproduces the experimental line profiles very well, we propose analytical expressions for practical use that approximate the calculated data between the density and temperature grid points.

Introducing dimensionless quantities  $\nu \equiv n_e/10^{24} \text{ m}^{-3}$  and  $\tau \equiv \log_2(T/4 \text{ eV})$ , the width and shift are given by

$$w = a_w \nu^{1/3} + b_w \nu^{2/3} + c_w \nu \quad (2)$$

and

$$d = a_d \nu^{b_d}, \quad (3)$$

respectively, with the temperature-dependent parameters

$$a_w = 11 + 4.5\tau - 0.5\tau^2, \quad (4a)$$

$$b_w = 52 - 0.84\tau + 3.1\tau^2, \quad (4b)$$

$$c_w = 28 + 1.9\tau - 1.5\tau^2, \quad (4c)$$

and

$$a_d = 8.0 - 0.44\tau + 0.09\tau^2, \quad (5a)$$

$$b_d = 0.924 + 0.018\tau. \quad (5b)$$

$a_w$ ,  $b_w$ ,  $c_w$ , and  $a_d$  are in units of  $\text{cm}^{-1}$ , and  $b_d$  is dimensionless. These formulas fit the width and shift data in Table II with better accuracy than 3% and 5%, respectively. The experimental widths and shifts from Table I are reproduced by these expressions within a 7% and 9% accuracy, respectively.

## VI. SUMMARY

Plasma broadening of the He II Paschen- $\alpha$  line has been studied for a long time. However, until recently, there had been significant disagreement, especially between the

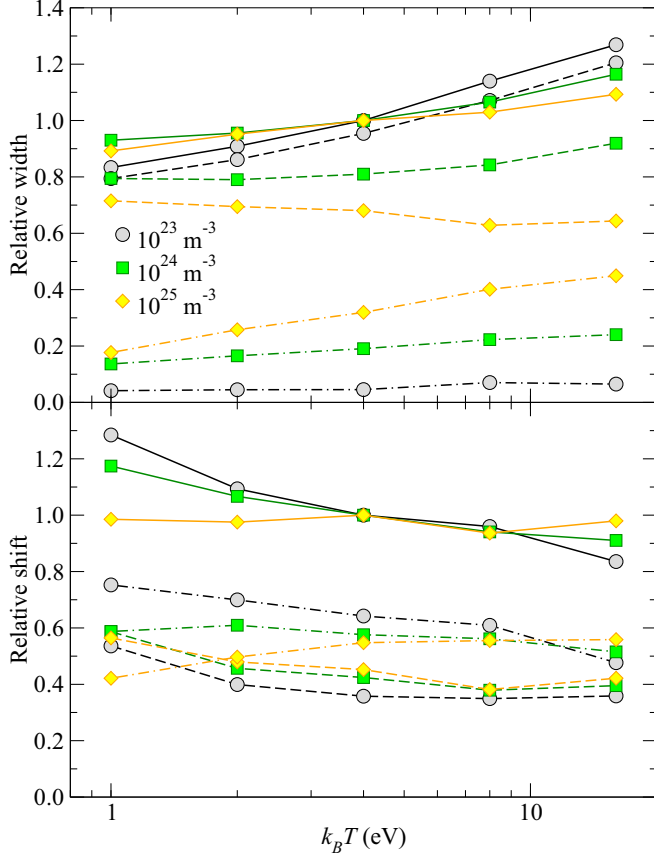


FIG. 6. Temperature dependence of the width (the upper panel) and the shift (the lower panel). Solid lines represent the total width (shift). The dashed and dotted-dashed lines correspond to contributions due to the  $\Delta n = 0$  (all poles with the penetration effects accounted for) and  $\Delta n \neq 0$  (only dipole) interaction terms. All values are normalized to those at  $k_B T = 4$  eV.

experimental and theoretical values of the line shift [1–6]. It was possible to reconcile the disagreement [7] by accounting for the full radiator-plasma interaction that included effects of the plasma perturbers penetrating the wave-function extent of the bound electron. In particular, the monopole radiator-plasma interaction term was found to be primarily responsible for the additional Stark shift that was missing in earlier calculations.

The present study investigated experimentally and theoretically the He II Paschen- $\alpha$  Stark profile over a wide range of electron densities and temperatures (varying by almost two and one orders of magnitude, respectively). For plasma diagnostics, the recently developed two-color Thomson scattering method [8] was used, with plasma parameters derived based on the electron or ion features of the measured TS spectra. Line-shift determination was greatly improved using a tunable Ti:sapphire cw laser with a second-harmonic generator and a wavemeter for absolute wavelength calibration.

As in the previous study, line-shape computer simulations [9] were performed for the plasma parameters derived. Very good agreement (about 5%) is found between the experimental and theoretical Stark widths and shifts for all spectra recorded. Additional calculations were performed to infer the

density and temperature dependences of the linewidth and line shift. Simple analytical expressions are suggested for plasma diagnostic applications that accurately approximate the calculated and measured data within the ranges of plasma parameters studied in this work.

#### ACKNOWLEDGMENTS

F.S. acknowledges the partial support of his work by the National Science Center Grant No. 2019/33/N/ST2/02823 and by the Polish Ministry of Science and Higher Education Grant No. 2020-N17/MNW/000010. The work of E.S. was partly supported by the University-of-Michigan multi-university Center of Excellence for Magnetic Acceleration, Compression, and Heating (U.S.).

#### APPENDIX: TRIVIAL CORRECTIONS

The data in Table II correspond to the normalized line shape  $L(\omega)$  widely used in line-broadening theory *without* the included photon kinematic and Boltzmann factors. On the other hand, what is measured in the experiment is

$$I(\omega) \propto L(\omega) \omega^m e^{-\hbar\omega/k_B T}, \quad (\text{A1})$$

where  $m$  is 3 or 4 if the instrument records the photon count or the radiative power spectrum, respectively. These nonlinear multiplicative factors cause line asymmetry, which is particularly important for determining the shift.

Corrections can be analytically evaluated under certain conditions. Radiation in the vicinity of the line center  $\omega_0$  is approximately

$$I(\omega) \propto L(\Delta\omega) \left[ 1 + \left( \frac{m}{\omega_0} - \frac{1}{k_B T} \right) \Delta\omega \right], \quad (\text{A2})$$

where  $\Delta\omega = \omega - \omega_0$  and assuming a sufficiently narrow line shape such that  $\Delta\omega \ll (\omega_0, k_B T)$ . Assuming further that the shape of the line core is close to a Lorentzian with the FWHM  $w$ , one readily obtains that the line peak is blueshifted by

$$\delta_1 = C_m w^2 / 8, \quad (\text{A3})$$

where

$$C_m = \frac{m}{\omega_0} - \frac{1}{k_B T}. \quad (\text{A4})$$

However, the line is not shifted as a whole; the further away from the center, the larger is the shift. In particular, the shift at the half of the line maximum is

$$\delta_{1/2} = C_m w^2 / 4, \quad (\text{A5})$$

i.e., twice as large. The relative importance of these shift corrections increases with density and temperature, reaching approximately 10% at the highest  $n_e$  and  $T$ .

Finally, conversion to the wavelength units introduces a similar asymmetry. Indeed,

$$I(\lambda) = I(\omega) \left| \frac{d\omega}{d\lambda} \right| \propto I(\omega) \omega^2. \quad (\text{A6})$$

In other words, one should use  $C_{m+2}$  instead of  $C_m$  in the corrections given by Eqs. (A4) and (A5) prior to the usual conversion of the Stark shift from the wave-number to wavelength units,  $d_\lambda = -\lambda_0^2 d$ .

- [1] C. Fleurier and P. L. Gall, *J. Phys. B: At. Mol. Phys.* **17**, 4311 (1984).
- [2] T. L. Pittman and C. Fleurier, *Phys. Rev. A* **33**, 1291 (1986).
- [3] R. Kobilarov, M. V. Popović, and N. Konjević, *Phys. Rev. A* **37**, 1021 (1988).
- [4] A. Gawron, J. D. Hey, X. J. Xu, and H.-J. Kunze, *Phys. Rev. A* **40**, 7150 (1989).
- [5] R. J. Peláez, C. Pérez, V. R. González, F. Rodríguez, J. A. Aparicio, and S. Mar, *J. Phys. B: At. Mol. Opt. Phys.* **38**, 2505 (2005).
- [6] C. Stollberg, E. Stambulchik, B. Duan, M. A. Gigosos, D. G. Herrero, C. A. Iglesias, and C. Mossé, *Atoms* **6**, 23 (2018).
- [7] F. Sobczuk, K. Dzierżęga, and E. Stambulchik, *Phys. Rev. E* **106**, L023202 (2022).
- [8] F. Sobczuk, K. Dzierżęga, W. Zawadzki, B. Pokrzywka, and E. Stambulchik, *Plasma Sources Sci. Technol.* **31**, 115012 (2022).
- [9] E. Stambulchik and C. A. Iglesias, *Phys. Rev. E* **105**, 055210 (2022).
- [10] E. Stambulchik and Y. Maron, *J. Quantum Spectrosc. Radiat. Transfer* **99**, 730 (2006).
- [11] S. Alexiou, *J. Quantum Spectrosc. Radiat. Transfer* **81**, 13 (2003).
- [12] K. Dzierżęga, A. Mendys, and B. Pokrzywka, *Spectrochim. Acta Part B* **98**, 76 (2014).
- [13] K. Dzierżęga, T. Pięta, W. Zawadzki, E. Stambulchik, M. Gavrilović-Božović, S. Jovičević, and B. Pokrzywka, *Plasma Sources Sci. Technol.* **27**, 025013 (2018).
- [14] K. Dzierżęga, F. Sobczuk, E. Stambulchik, and B. Pokrzywka, *Phys. Rev. E* **103**, 063207 (2021).
- [15] E. Stambulchik and Y. Maron, *J. Quantum Spectrosc. Radiat. Transfer* **315**, 108889 (2024).
- [16] H. R. Griem, *Spectral Line Broadening by Plasmas* (Academic Press, New York, 1974).
- [17] E. Stambulchik and A. V. Demura, *J. Phys. B: At. Mol. Opt. Phys.* **49**, 035701 (2016).
- [18] This is true for the degenerate atomic models. However, the increasing contribution of the ion-induced quadratic Stark effect maintains a positive temperature dependence.